Available online at www.sciencedirect.com
SCIENCE DIRECT®
International Journal of Multiphase Flow 31 (2005) 492–513
International Journal of Multiphase Flow
www.elsevier.com/locate/ijmulflow

Sliding of fine particles on the slip surface of rising gas bubbles: Resistance of liquid shear flows

Anh V. Nguyen *, Graeme J. Jameson

Discipline of Chemical Engineering and Special Research Centre for Multiphase Processes, The University of Newcastle, Callaghan, New South Wales 2308, Australia

Received 17 October 2003; received in revised form 10 January 2005

Abstract

In this paper a model was developed to describe the shear flow resistance force and torque acting on a fine particle as it slides on the slip surface of a rising gas bubble. The shear flow close to the bubble surface was predicted using a Taylor series and the numerical data obtained from the Navier–Stokes equations as a function of the polar coordinates at the bubble surface, the bubble Reynolds number, and the gas hold-up. The particle size was considered to be sufficiently small relative to the bubble size that the bubble surface could be locally approximated to a planar interface. The Stokes equation for the disturbance shear flows was solved for the velocity components and pressure using series of bispherical coordinates and the boundary conditions at the no-slip particle surface and the slip bubble surface. The solutions for the disturbance flows were then used to calculate the flow resistance force and torque on the particle as a function of the separation distance between the bubble and particle surfaces. The resistance functions were determined by dividing the actual force and torque by the corresponding (Stokes) force and torque in the bulk phase. Finally, numerical and simplified analytical rational approximate solutions for force correction factors for sliding particles as a function of the (whole range of the) separation distance are presented, which are in good agreement with the exact numerical result and can be readily applied to more general modelling of the bubble–particle interactions.

* Corresponding author. Tel.: +61 249216189; fax: +61 249216920.
E-mail address: anh.nguyen@newcastle.edu.au (A.V. Nguyen).

0301-9322/$ - see front matter © 2005 Elsevier Ltd. All rights reserved.
doi:10.1016/j.ijmultiphaseflow.2005.01.005

Keywords: Drag force and torque; Stokes correction factor; Particle–flow interaction; Bubble–particle interaction; Gas–liquid–solid multiphase flow systems

1. Introduction

Interaction between fine solid particles and rising air bubbles in water is critical to the collection of hydrophobic (water-repellent) particles in froth flotation which is widely used in the mineral and coal processing industry (Jameson et al., 1977; Schulze, 1983). The bubble–particle collection interaction involves a number of steps, which are usually divided into three main groups, namely, the collision (encounter), attachment and detachment interactions. The bubble–particle collision determines the efficiency of the bubble–particle encounter on the basis of the physics of the particle and bubble motions and hydrodynamics of liquid flow, and has been studied most extensively (Dai et al., 2000; Dobby and Finch, 1987; Jameson et al., 1977; Nguyen, 1999; Schulze, 1989). Both the attachment and detachment interactions strongly depend on the interfacial properties of the particle–water and bubble–water interfaces, as well as the hydrodynamic forces operating at very short separation distances, which are of the order of the thickness of the thin intervening liquid films between the bubble and the particles.

During the encounter interaction, the particle's approach to the bubble is influenced by the Stokes drag force: $\mathbf{F} = -6\pi\mu R(\mathbf{V} - \mathbf{W})$, where R is the particle radius, μ is the liquid viscosity, and $\mathbf{V}$ and $\mathbf{W}$ are the vectors of the particle and fluid velocities, respectively. When the particle approaches the bubble surface with an intervening liquid film, the hydrodynamic resistance increases rapidly. This deviation of the hydrodynamic resistance is due to the liquid film and can be accounted for using the hydrodynamic resistance functions. The Stokes drag force is modified to give

- In the (radial) direction of the bubble–particle centreline:

$$F_{\mathrm{r}} = -6\pi\mu R V_{\mathrm{r}} f_1 + 6\pi\mu R W_{\mathrm{r}} f_2 \tag{1}$$

- In the (tangential) direction perpendicular to the centreline:

$$F_{\theta} = -6\pi\mu R V_{\theta} f_3 + 6\pi\mu R W_{\theta} f_4 \tag{2}$$

where the subscript 'r' and 'θ' describe the radial and tangential components of the drag force and the particle and fluid velocities, respectively, as shown in Fig. 1, and functions f_i ($i = 1$–4) describe the hydrodynamic resistance functions. For the interaction between a solid particle and a solid surface, all the four hydrodynamic resistance functions are available as a function of the separation distance between the particle and the solid surface (Goldman et al., 1967a,b; Goren and O'Neill, 1971; Happel and Brenner, 1965a). For the interaction between a solid particle and an air bubble, where the tangential velocity component is non-zero, the surface will be described a "slip surface", and the following hydrodynamic resistance functions are available as a function of the separation distance: f_1, f_2 (Nguyen and Evans, 2002) and f_3 (Nguyen and Evans, 2004).

The aim of this paper is derive the exact solution for the hydrodynamic resistance function f_4 for the interaction between a solid particle and an air bubble with a slip surface, which can be used

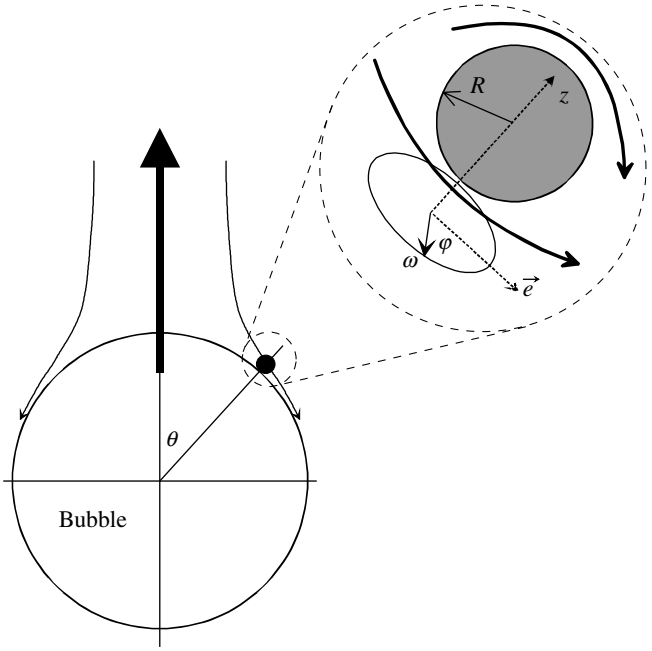

Fig. 1. Spherical particle with radius R in the close proximity to the slip surface of a rising bubble. The flow field passing the particle comprises the shear (inset) and axisymmetric stagnation flows in the directions tangential and normal to the bubble surface, respectively. The local cylindrical coordinate system (ω, φ, z) is used to model the disturbance flow.

in the modelling of the bubble–particle attachment in froth flotation. We reasonably assume that the particle size (which is typically of the order of 10 μm) in flotation is significantly smaller than the size of air bubbles (which is typically of the order of 1 mm) so that the local geometry of the particle–bubble surface can be approximated to the particle–planar surface geometry. We also focus on the case when the deformation of the gas–liquid interface due to the particle–bubble interaction is insignificant. This is particularly true for the particle sliding motion over the bubble surface and significantly simplifies the analysis presented in this paper. Further aspects of the bubble deformation will be given in the discussion. Furthermore, it can be assumed that the undisturbed-by-the-particle flow of liquid close to the bubble surface is a creeping flow, and, thus, it can be decomposed into two independent additive flows, namely, the flows normal and tangential to the bubble surface, due to the linearity of the governing Stokes equations. The former flow is therefore a stagnation flow while the latter flow is a cross shear flow. Figs. 1 and 2 show the shear flow needed in developing the hydrodynamic resistance function f_4.

2. The shear flow close to the slip surface of an rising air bubble

It is required to quantify the velocity W_0 (in the second term of Eq. (2)) of the shear flow of the liquid close to the slip surface of the bubble in the absence of the particle. For the sake of simplicity, the subscript "θ" associated with the shear flow will be dropped hereafter.

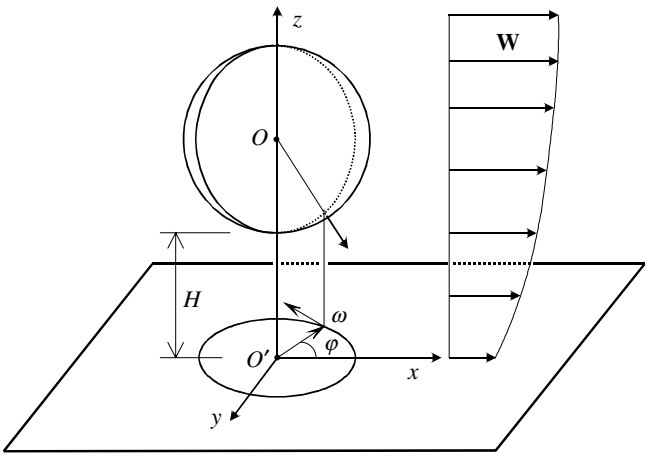

Fig. 2. Particle (stationary relative to the interface) in the shear flow parallel to a slip planar gas–liquid interface and the local cylindrical coordinates (ω, φ, z). The shown parabolic profile for the undisturbed velocity satisfies the condition of zero stress in the global spherical coordinates with the origin located at the bubble centre in Fig. 1, which gives $\mathrm{d}W/\mathrm{d}r - W = 0$ at $r = R_b$.

For air bubbles with very low Reynolds numbers, the shear flow can be predicted from the Hadamard–Rybczynski solution, which gives (Clift et al., 1978):

$$W(r,\theta) = U\left\{1 - \frac{2+3\kappa}{4+4\kappa}\frac{R_b}{r} - \frac{\kappa}{4+4\kappa}\left(\frac{R_b}{r}\right)^3\right\}\sin\theta \tag{3}$$

where κ is the ratio of the air to water viscosities, r and θ are the radial and polar coordinates measured from the bubble centre (Fig. 1). R_b and U are the bubble radius and slip velocity, respectively. Since $\kappa \ll 1$, Eq. (3) can be simplified to

$$W(r,\theta) = U\left\{1 - \frac{R_b}{2r}\right\}\sin\theta \tag{4}$$

The potential flow has also been used to model the shear flow on air bubbles, giving

$$W(r,\theta) = U\left\{1 + \frac{1}{2}\left(\frac{R_b}{r}\right)^3\right\}\sin\theta \tag{5}$$

This solution is, strictly speaking, valid for inviscid liquids. However, all real liquids have non-zero viscosity so that the concept of an inviscid liquid and the potential flow are an idealization. Nevertheless, the potential flow can be a useful reference point for real liquid flows at high Reynolds number. For example, at high Reynolds number, viscous effects may be insignificant in the large region of the flow field which is far from the bubble surface. These regions may be treated as if the liquid were inviscid. In the boundary layer adjacent to the bubble surface, the effect of viscosity must be considered. In the boundary layer theory, the derivatives with respect to the

streamwise coordinate are usually neglected, relative to those in the transverse direction, leading to (Moore, 1963)

$$\frac{W(r,\theta)}{U} = \left\{1 + \frac{1}{2}\left(\frac{R_b}{r}\right)^2\right\}\sin\theta - \frac{4(1-\cos\theta)\sqrt{2+\cos\theta}}{\sqrt{Re}\sin\theta} f\left\{\frac{3(r/R_b-1)\sqrt{Re}/4}{(1-\cos\theta)\sqrt{2+\cos\theta}}\right\} \tag{6}$$

where the function f is described by $f(y) \equiv \exp(-y^2)/\sqrt{\pi} - y\,\mathrm{erfc}(y)$ and $\mathrm{erfc}(y)$ is the complementary error function. The bubble Reynolds number is $Re = 2\delta R_b U/\mu$, where δ and μ are the liquid density and viscosity. The first term in Eq. (6) is the velocity of the shear flow predicted by Eq. (5) from the potential flow theory. Since the boundary layer thickness is proportional to $1/\sqrt{Re}$, the boundary layer theory is less accurate for low Reynolds numbers. Quantitatively, our numerical results (Nguyen, 1999) obtained from the Navier–Stokes equations using the CFD code FLUENT show that Eq. (6) is accurate if $Re > 150$.

For $150 > Re > 1$, no analytical solution for $W(r,\theta)$ is available. However, the shear flow close to the bubble surface at the intermediate Reynolds numbers can be empirically described using a Taylor series by (Nguyen, 1994, 1999)

$$W(r,\theta) = (W)_{r=R_b} + (r-R_b)\left(\frac{\partial W}{\partial r}\right)_{r=R_b} + \frac{(r-R_b)^2}{2}\left(\frac{\partial^2 W}{\partial r^2}\right)_{r=R_b} + \mathrm{O}\left\{(r-R_b)^3\right\} \tag{7}$$

In this equation, the velocity and its derivatives at the bubble surface can be determined from the numerical data for the surface velocity, surface vorticity and surface pressure, obtained from the numerical computation solution to the Navier–Stokes equation. For a slip bubble surface, the surface velocity in Eq. (7) is non-zero and describes the uniform component of the shear flow, while the other two terms on the right-hand side of Eq. (7) describe the linear and parabolic components of the shear flows, respectively. The rational approximation based on the asymptotic analysis for the low and high Reynolds numbers flows described by Eqs. (4) and (6) can be used to describe the numerical data the surface velocity and its derivatives, leading to the following prediction for the required shear flow

$$\frac{W(r,\theta)}{U} = \frac{r}{R_b}\frac{(X + Y\cos\theta)\sin\theta}{2} + \left(\frac{r}{R_b} - 1\right)^2 \frac{(M + N\cos\theta)\sin\theta}{2} + \mathrm{O}\left\{(r-R_b)^3\right\} \tag{8}$$

where the model parameters X, Y, M and N are functions of the bubble Reynolds number, as well as the gas hold-up. These functions are described in the literature (Nguyen, 1999).

It is important to note that Eq. (8) is empirically developed from the full numerical results for the leading hemispherical surface (i.e. $0 \leqslant \theta \leqslant \pi/2$) of the rising bubbles only. Consequently, the equation should not be applied in instances where flow field over the entire surface of the bubble is required, for example, in the drag force determination. This is especially the case when the rear surface of the bubble is likely to be immobile, such as when surfactants or other impurities are present in the liquid. The inclusion of the second-order term in Eq. (8) for the undisturbed shear flow is also important since the first-order prediction is usually poor for the modelling of the particle–bubble attachment interaction (Dobby and Finch, 1986; Nguyen, 1993). In the following, Eq. (8) for the shear flow velocity as a function of the radial coordinate will be used to derive the local disturbance flow by the presence of the particle.

3. Governing equations for the local disturbance flow

The local cylindrical coordinate system (ω, φ, z), as shown in Figs. 1 and 2, is used to describe the shear flow which is locally disturbed by the particle. The origin of the system is located at the intersection between the bubble–particle centreline and the bubble surface. The z-axis passes through the centre of the particle, while the ω and φ axes lies on the plane tangential to the bubble surface. To predict the resistance function f_4 for the liquid flow in Eq. (2), the solid sphere is assumed stationary in a shear flow at a distance H from a slip gas–liquid interface. For the local disturbance liquid flow the equations of momentum and continuity in the cylindrical coordinates (ω, φ, z), with the corresponding velocity components (w_ω, w_φ, w_z) and pressure p can be described by

$$\frac{\partial}{\partial\omega}\left(\frac{p}{\mu}\right) = \nabla^2 w_\omega - \frac{w_r}{\omega^2} - \frac{2}{\omega^2}\frac{\partial w_\varphi}{\partial\varphi} \tag{9}$$

$$\frac{1}{\omega}\frac{\partial}{\partial\varphi}\left(\frac{p}{\mu}\right) = \nabla^2 w_\varphi - \frac{w_\varphi}{\omega^2} + \frac{2}{\omega^2}\frac{\partial w_\omega}{\partial\varphi} \tag{10}$$

$$\frac{\partial}{\partial z}\left(\frac{p}{\mu}\right) = \nabla^2 w_z \tag{11}$$

$$\frac{1}{\omega}\frac{\partial(\omega w_\omega)}{\partial\omega} + \frac{1}{\omega}\frac{\partial w_\varphi}{\partial\varphi} + \frac{\partial w_z}{\partial z} = 0 \tag{12}$$

In these equations, the Laplace operator is defined by

$$\nabla^2 \equiv \frac{\partial^2}{\partial\omega^2} + \frac{1}{\omega}\frac{\partial}{\partial\omega} + \frac{1}{\omega^2}\frac{\partial^2}{\partial\varphi^2} + \frac{\partial^2}{\partial z^2} \tag{13}$$

4. Boundary conditions for the local disturbance shear flow

In terms of the local cylindrical coordinate system (ω, φ, z), as shown in Fig. 2, the velocity of the undisturbed shear flow given by Eq. (8) can be rewritten as a function of z by

$$\vec{W} = U\sum_{l=0}^{2} G_l (z/R)^l \vec{e} \tag{14}$$

where $z = r - R_b$ and is the dimensional distance (coordinate) measured from the interface, $\vec{e}$ is the unit vector in the direction tangential to the bubble surface (Fig. 1), and G_l's are functions of the polar coordinate, θ, and the bubble model parameters X, Y, M and N. Furthermore, because of the linearity of the Stokes equations and the shear flow described by Eq. (7), without loss of generality we can consider the basic undisturbed flow which can be mathematically described by

$$\vec{W} = UG_l(z/R)^l\vec{e} \tag{15}$$

The tangential unit vector in the cylindrical coordinates yields $\vec{e} = \vec{e}_\omega \cos\varphi - \vec{e}_\varphi \sin\varphi$ (Fig. 2), allowing the cylindrical components of the shear flow velocity to be described by

$$W_\omega = \left(\frac{z}{R}\right)^l UG_l \cos\varphi \tag{16}$$

$$W_\varphi = -\left(\frac{z}{R}\right)^l UG_l \sin\varphi \tag{17}$$

$$W_z = 0 \tag{18}$$

The first boundary condition for the velocity of the disturbance flow by the presence of the particle can be derived from the fact that far from the particle surface the flow disturbance does not occur, and the undisturbed and disturbance flow velocities must be the same, leading to:

$$\vec{w}(\infty) = \vec{W} \tag{19}$$

The boundary conditions applied at the particle surface can be described by

$$\vec{w} = 0 \tag{20}$$

In the cylindrical coordinates, Eq. (19) for the far field boundary conditions gives

$$w_\omega(\infty) = \left(\frac{z}{R}\right)^l UG_l \cos\varphi \tag{21}$$

$$w_\varphi(\infty) = -\left(\frac{z}{R}\right)^l UG_l \sin\varphi \tag{22}$$

$$w_z(\infty) = 0 \tag{23}$$

5. Method and solution for the local disturbance shear flow

In the cylindrical coordinates shown in Fig. 2, the solutions for the velocity components and the pressure of the disturbed flow can be simplified by employing the following transformations:

$$w_\omega = \left\{\beta + \left(\frac{z}{R}\right)^l\right\} UG_l \cos\varphi \tag{24}$$

$$w_\varphi = \left\{\gamma - \left(\frac{z}{R}\right)^l\right\} UG_l \sin\varphi \tag{25}$$

$$w_z = \varepsilon UG_l \cos\varphi \tag{26}$$

$$p = \lambda\mu UG_l \cos\varphi \tag{27}$$

where β, γ, ε and λ are functions of ω and z only. Substituting Eqs. (24)–(27) into Eqs. (9)–(12), the governing equations become:

$$\frac{\partial\lambda}{\partial\omega} = L_0^2(\beta) - \frac{\beta + 2\gamma}{\omega^2} \tag{28}$$

$$\frac{\lambda}{\omega} = -L_0^2(\gamma) + \frac{2\beta + \gamma}{\omega^2} \tag{29}$$

$$\frac{\partial\lambda}{\partial z} = L_0^2(\varepsilon) \tag{30}$$

$$\frac{\partial\beta}{\partial\omega} + \frac{\beta + \gamma}{\omega} + \frac{\partial\varepsilon}{\partial z} = 0 \tag{31}$$

In these equations, L_0^2 describes one of the differential operators L_m^2 for $m = 0$, 1, and 2, defined by

$$L_m^2 \equiv \frac{\partial^2}{\partial\omega^2} + \frac{1}{\omega}\frac{\partial}{\partial\omega} - \frac{m^2}{\omega^2} + \frac{\partial^2}{\partial z^2} \tag{32}$$

The solution of the linear differential equations (28)–(30) can be expressed by the following equations:

$$\beta = \frac{\omega\lambda}{2} + \frac{\alpha_0 + \alpha_2}{2} \tag{33}$$

$$\gamma = \frac{\alpha_2 - \alpha_0}{2} \tag{34}$$

$$\varepsilon = \frac{z\lambda}{2} + \alpha_1 \tag{35}$$

where α_m satisfies the differential equation $L_m^2(\alpha_m) = 0$ for $m = 0$, 1, and 2, and has the following solution (Batchelor, 1972)

$$\alpha_m = (\cosh\xi - \cos\eta)^{1/2}\sin^m\eta \sum_{n=m}^{\infty} [C_{m,n}\cosh(q_n\xi) + S_{m,n}\sinh(q_n\xi)]P_n^{(m)}(\cos\eta) \tag{36}$$

where $C_{m,n}$ and $S_{m,n}$ are the integration constants. $P_n^{(m)}(\cos\eta)$ describes the mth derivative of the Legendre polynomial $P_n(\cos\eta)$ of order n with respect to $\cos\eta$. This derivative is also described by P_n' and P_n'' for $m = 1$ and 2, respectively. For $m = 0$, the derivative is simply the Legendre polynomial. q_n in Eq. (36) is a function of the summation index n and is defined by

$$q_n = \frac{2n + 1}{2} \tag{37}$$

In Eq. (36), ξ and η are the bispherical coordinates, which are linked to the cylindrical coordinates (ω, z) by

$$\omega = \frac{c\sin\eta}{\cosh\xi - \cos\eta} \tag{38}$$

$$z = \frac{c\sinh\xi}{\cosh\xi - \cos\eta} \tag{39}$$

where c is a constant determined by applying Eqs. (38) and (39) at the particle surface, $\xi = \tau$. We obtain

$$c = R\sinh\tau \tag{40}$$

The solution for λ can be obtained by substituting the solution for α_m ($m = 1$, 2 and 3), described by Eq. (36), into Eqs. (33) and (35). Inserting the obtained result into Eq. (29) gives, after a little algebra,

$$\lambda = (\cosh\xi - \cos\eta)^{1/2}\frac{\sin\eta}{c}\sum_{n=1}^{\infty}[C_{\lambda,n}\cosh(q_n\xi) + S_{\lambda,n}\sinh(q_n\xi)]P_n'(\cos\eta) \tag{41}$$

6. Solutions for the integration constants

The integration constants $C_{m,n}$ to $S_{m,n}$ ($m = 0, 1$ and 2) in Eqs. (36), and $C_{\lambda,n}$ and $S_{\lambda,n}$ in (41) can be determined from the boundary conditions applied at both the particle surface and the gas–liquid interface.

6.1. Slip gas–liquid interface

At the gas–liquid interface the velocity component normal to the interface vanishes, i.e.

$$w_z(z = 0) = 0 \tag{42}$$

However, as there is slip at the gas–liquid interface, the other two velocity components at the interface are non-zero, and the tangential stresses are zero, leading to

$$\left(\frac{\partial w_\omega}{\partial z}\right)_{z=0} = 0 \tag{43}$$

$$\left(\frac{\partial w_\varphi}{\partial z}\right)_{z=0} = 0 \tag{44}$$

These boundary conditions can be used to find the solutions for α_0, α_1, α_2 and λ for the disturbance flow from Eqs. (24)–(27) and (33)–(35). We can obtain

$$\alpha_1(z = 0) = 0 \tag{45}$$

$$\frac{c\sin\eta}{1-\cos\eta}\left(\frac{\partial\lambda}{\partial z}\right)_{z=0} + \left(\frac{\partial\alpha_0}{\partial z}\right)_{z=0} + \left(\frac{\partial\alpha_2}{\partial z}\right)_{z=0} + \left(\frac{\partial}{\partial z}\left\{\frac{z}{R}\right\}^l\right)_{z=0} = 0 \tag{46}$$

$$\left(\frac{\partial\alpha_0}{\partial z}\right)_{z=0} - \left(\frac{\partial\alpha_2}{\partial z}\right)_{z=0} - \left(\frac{\partial}{\partial z}\left\{\frac{z}{R}\right\}^l\right)_{z=0} = 0 \tag{47}$$

where $(\partial z^l/\partial z)_{z=0} = 0$ for $l = 0$ and 2, while $(\partial z^l/\partial z)_{z=0} = 1$ for $l = 1$.

6.2. Particle surface

At the particle surface, $\xi = \tau$, and the boundary conditions described by Eq. (20) give:

$$\frac{\lambda c \sin\eta}{\cosh\tau - \cos\eta} + \alpha_0 + \alpha_2 = -2\left(\frac{\sinh^2\tau}{\cosh\tau - \cos\eta}\right)^l \tag{48}$$

$$\alpha_2 - \alpha_0 = 2\left(\frac{\sinh^2\tau}{\cosh\tau - \cos\eta}\right)^l \tag{49}$$

$$\frac{\lambda c \sinh\tau}{\cosh\tau - \cos\eta} + 2\alpha_1 = 0 \tag{50}$$

6.3. Additional boundary conditions

The solutions described by Eqs. (36) and (41) contain eight unknown integration constants, but the velocity-component boundary conditions applied at the gas–liquid interface and the particle surface give rise to only six equations, viz. Eqs. (45)–(50). Two more equations are required and can be obtained from the equation of continuity, described by Eq. (31), applied at the interface and the particle surface, giving

$$\left(3\lambda + \omega\frac{\partial\lambda}{\partial\omega} + z\frac{\partial\lambda}{\partial z} + \frac{\partial\alpha_2}{\partial\omega} + \frac{\alpha_2}{\omega} + \frac{\partial\alpha_0}{\partial\omega} + 2\frac{\partial\alpha_1}{\partial z}\right)_{\xi=0 \text{ or } \tau} = 0 \tag{51}$$

The derivation of the remaining unknown equation is presented later after some solutions for the integration constants are available.

6.4. Algebraic equations for the integration constants

When $z = 0$, Eq. (39) gives $\xi = 0$. Therefore, the boundary condition given by Eq. (45) applied at the plane $z = 0$ yields

$$C_{1,n} = 0 \quad \text{for all } n \tag{52}$$

The solution given by Eq. (36) for α_1 simplifies to

$$\alpha_1 = (\cosh\xi - \cos\eta)^{1/2} \sin\eta \sum_{n=1}^{\infty} S_{1,n} \sinh(q_n\xi) P_n^{(m)}(\cos\eta) \tag{53}$$

6.4.1. Boundary condition equations at the gas–liquid interface

Both Eqs. (46) and (47) gives

$$2\left(\frac{\partial\alpha_0}{\partial z}\right)_{z=0} = 2\left(\frac{\partial\alpha_2}{\partial z}\right)_{z=0} + 2\left(\frac{\partial}{\partial z}\left\{\frac{z^l}{R}\right\}\right)_{z=0} = -\frac{c\sin\eta}{1-\cos\eta}\left(\frac{\partial\lambda}{\partial z}\right)_{z=0}$$

These dependencies can be applied as follows:

(A) Inserting the solutions for α_0 and λ into the first equation: $2(\frac{\partial\alpha_0}{\partial z})_{z=0} = -\frac{c\sin\eta}{1-\cos\eta}(\frac{\partial\lambda}{\partial z})_{z=0}$ gives

$$\sum_{n=0}^{\infty} 2S_{0,n} \times (1-\cos\eta)P_n(\cos\eta) + \sum_{n=1}^{\infty} S_{\lambda,n} \times \sin^2\eta P'_n(\cos\eta) = 0 \tag{54}$$

We have the following recurrence relations (Magnus et al., 1966)

$$\sin^2\eta P'_n(\cos\eta) = \frac{n(n+1)}{2n+1}[P_{n-1}(\cos\eta) - P_{n+1}(\cos\eta)]$$

$$\cos\eta P_n(\cos\eta) = \frac{(n+1)P_{n+1}(\cos\eta) + nP_{n-1}(\cos\eta)}{2n+1}$$

Applying these recurrence relations we obtain from Eq. (54)

$$\sum_{n=0}^{\infty} S_{0,n}2\left\{P_n(\cos\eta) - \frac{(n+1)P_{n+1}(\cos\eta) + nP_{n-1}(\cos\eta)}{2n+1}\right\} + \sum_{n=1}^{\infty} S_{\lambda,n}\frac{n(n+1)}{2n+1}[P_{n-1}(\cos\eta) - P_{n+1}(\cos\eta)] = 0 \tag{55}$$

Rearranging gives

$$\sum_{n=0}^{\infty} P_{n+1}(\cos\eta)\{-(2n+2)S_{0,n} - (n^2+n)S_{\lambda,n}\} + P_n(\cos\eta)(4n+2)S_{0,n} + P_{n-1}(\cos\eta)\{-2nS_{0,n} + (n^2+n)S_{\lambda,n}\} = 0$$

Finally, equating terms with the same order of the Legendre polynomials we obtain

$$-2nS_{0,n-1} + (4n+2)S_{0,n} - (2n+2)S_{0,n+1} - (n^2-n)S_{\lambda,n-1} + (n^2+3n+2)S_{\lambda,n+1} = 0 \tag{56}$$

This equation represents one of the required algebraic equations for determining the integration constants.

(B) Using the second equation: $2(\frac{\partial\alpha_2}{\partial z})_{z=0} + 2(\frac{\partial}{\partial z}\{\frac{z^l}{R}\})_{z=0} = -\frac{c\sin\eta}{1-\cos\eta}(\frac{\partial\lambda}{\partial z})_{z=0}$ gives

$$2(1-\cos\eta)\sum_{n=2}^{\infty} S_{2,n}P''_n(\cos\eta) + \frac{2X_n}{(1-\cos\eta)^{1/2}} + \sum_{n=1}^{\infty} S_{\lambda,n}P'_n(\cos\eta) = 0 \tag{57}$$

where $X_n = \begin{cases} 0 \text{ for } l = 0 \text{ and } 2 \\ \sinh\tau \text{ for } l = 1 \end{cases}$

To solve Eq. (57) the following recurrence relations (Magnus et al., 1966) can be employed:

$$P'_n(\cos\eta) = \frac{P''_{n+1}(\cos\eta) - P''_{n-1}(\cos\eta)}{2n+1}$$

$$\cos\eta P''_n(\cos\eta) = \frac{(n-1)P''_{n+1}(\cos\eta) + (n+2)P''_{n-1}(\cos\eta)}{2n+1}$$

$$(1-\cos\eta)^{-1/2} = \sqrt{2}\sum_{n=0}^{\infty} P_n(\cos\eta)$$
$$= \sqrt{2}\sum_{n=2}^{\infty} \frac{P''_{n+2}(\cos\eta)}{(2n+3)(2n+1)} - \frac{2P''_n(\cos\eta)}{(2n+3)(2n-1)} + \frac{P''_{n-2}(\cos\eta)}{(2n+1)(2n-1)}$$

leading to

$$\frac{-(2n-4)S_{2,n-1}+S_{\lambda,n-1}}{2n-1} + 2S_{2,n} - \frac{(2n+6)S_{2,n+1}+S_{\lambda,n+1}}{2n+3} = \frac{-96\sqrt{2}X_n}{45-72n-56n^2+32n^3+16n^4} \tag{58}$$

This equation represents another required algebraic equation for the integration constants.

6.4.2. Continuity equation applied at the gas–liquid and liquid–solid interfaces

Inserting the solutions for α_0, α_1, α_2 and λ into the continuity equation, Eq. (51), applied at the gas–liquid and liquid–solid interfaces and following similar procedure used to obtain the required equations, Eqs. (56) and (58), gives, respectively,

$$-S_{0,n-1}+2S_{0,n}-S_{0,n+1}+(n^2-3n+2)S_{2,n-1}-(2n^2+2n-4)S_{2,n}+(n^2+5n+6)S_{2,n+1} + 5S_{\lambda,n-1}-(n-1)S_{\lambda,n}+(n+2)S_{\lambda,n+1}=0 \tag{59}$$

$$-C_{0,n-1}+2C_{0,n}-C_{0,n+1}+(n^2-3n+2)C_{2,n-1}-(2n^2+2n-4)C_{2,n}+(n^2+5n+6)C_{2,n+1} + 5C_{\lambda,n-1}-(n-1)C_{\lambda,n}+(n+2)C_{\lambda,n+1}+(2-2n)S_{1,n-1}+(4n+2)S_{1,n}-(2n+4)S_{1,n+1}=0 \tag{60}$$

6.4.3. Numerical solutions for S_0, S_2 and S_λ

Three equations, Eqs. (56), (58) and (59) for S_0, S_2 and S_λ can be solved for a given value of H. To do this, it is firstly realized that $S_{0,n+1}=0$, $S_{2,n+1}=0$ and $S_{\lambda,n+1}=0$ on the basis that the series $S_{0,n+1}$, $S_{2,n+1}$ and $S_{\lambda,n+1}$ converge to zero if the summation index n is significantly large. The significant solution of the remaining linear equations containing the unknown integration constants can be solved numerically. The numerical solutions show that $S_{0,n}=S_{2,n}=S_{\lambda,n}=0$ for all n. These solutions significantly simplify the analysis for the remaining unknown integration constants, which is described below.

6.4.4. Boundary condition equations at the particle surface

Solving the boundary condition equations, Eqs. (48)–(50), at the particle surface gives:

$$(\alpha_0)_{\xi=\tau} = (\alpha_1)_{\xi=\tau}\frac{\sin\eta}{\sinh\tau} - 2\left(\frac{\sinh^2\tau}{\cosh\tau-\cos\eta}\right)^l \tag{61}$$

$$(\alpha_2)_{\xi=\tau} = (\alpha_1)_{\xi=\tau}\frac{\sin\eta}{\sinh\tau} \tag{62}$$

$$(\lambda)_{\xi=\tau} = -2(\alpha_1)_{\xi=\tau}\frac{\cosh\tau - \cos\eta}{c\sinh\tau} \tag{63}$$

Inserting the appropriate solutions into Eqs. (61)–(63) lead to

$$\sum_{n=0}^{\infty} C_{0,n}\cosh(q_n\tau)P_n(\cos\eta) = \frac{\sin^2\eta}{\sinh\tau}\sum_{n=1}^{\infty} S_{1,n}\sinh(q_n\tau)P'_n(\cos\eta) - \frac{2\sinh^{2l}\tau}{(\cosh\tau-\cos\eta)^{l+1/2}} \tag{64}$$

$$\sum_{n=2}^{\infty} C_{2,n}\cosh(q_n\tau)P''_n(\cos\eta) = \frac{1}{\sinh\tau}\sum_{n=1}^{\infty} S_{1,n}\sinh(q_n\tau)P'_n(\cos\eta) \tag{65}$$

$$\sum_{n=1}^{\infty} C_{\lambda,n}\cosh(q_n\tau)P'_n(\cos\eta) + 2\frac{\cosh\tau-\cos\eta}{\sinh\tau}\sum_{n=1}^{\infty} S_{1,n}\sinh(q_n\tau)P'_n(\cos\eta) = 0 \tag{66}$$

The following recurrence relations can be used to solve Eqs. (64) and (65):

$$\sin^2\eta P'_n(\cos\eta) = \frac{n(n+1)}{2n+1}[P_{n-1}(\cos\eta) - P_{n+1}(\cos\eta)]$$

$$P'_n(\cos\eta) = \frac{P''_{n+1}(\cos\eta) - P''_{n-1}(\cos\eta)}{2n+1}$$

$$\cos\eta P'_n(\cos\eta) = \frac{(n+1)P'_{n-1}(\cos\eta) + nP'_{n+1}(\cos\eta)}{2n+1}$$

$$(\cosh\tau-\sigma)^{-1/2} = \sqrt{2}\sum_{n=0}^{\infty} P_n(\sigma)\exp(-q_n\tau)$$

$$\frac{\sinh\tau}{(\cosh\tau-\sigma)^{3/2}} = 2\sqrt{2}\sum_{n=0}^{\infty} P_n(\sigma)q_n\exp(-q_n\tau)$$

$$\frac{\sinh^2\tau}{(\cosh\tau-\sigma)^{5/2}} = \frac{4\sqrt{2}}{3}\sum_{n=0}^{\infty} P_n(\sigma)q_n(q_n+\coth\tau)\exp(-q_n\tau)$$

Equating terms in Eqs. (64) and (65) with the same Legendre polynomials we obtain

$$C_{0,n} = \left\{-S_{1,n-1}\frac{n^2-n}{2n-1}\frac{\sinh(q_{n-1}\tau)}{\sinh\tau} + S_{1,n+1}\frac{n^2+3n+2}{2n+3}\frac{\sinh(q_{n+1}\tau)}{\sinh\tau} - Y_n\right\}\operatorname{sech}(q_n\tau) \tag{67}$$

$$C_{2,n} = \left\{S_{1,n-1}\frac{\sinh(q_{n-1}\tau)}{(2n-1)\sinh\tau} - S_{1,n+1}\frac{\sinh(q_{n+1}\tau)}{(2n+3)\sinh\tau}\right\}\operatorname{sech}(q_n\tau) \tag{68}$$

$$C_{\lambda,n} = \left\{S_{1,n-1}\frac{\sinh(q_{n-1}\tau)}{\sinh\tau}\frac{2n-2}{2n-1} - S_{1,n}2\sinh(q_n\tau)\coth\tau + S_{1,n+1}\frac{\sinh(q_{n+1}\tau)}{\sinh\tau} + \frac{2n+4}{2n+3}\right\}\operatorname{sech}(q_n\tau) \tag{69}$$

where

$$Y_n = \begin{cases} 2\sqrt{2}\exp(-q_n\tau) & \text{for } l = 0 \\ 4\sqrt{2}q_n\exp(-q_n\tau)\sinh\tau & \text{for } l = 1 \\ (8\sqrt{2}/3)q_n(q_n+\coth\tau)\exp(-q_n\tau)\sinh^2\tau & \text{for } l = 2 \end{cases}$$

Eqs. (67)–(69) can be substituted into the continuity Eq. (60), resulting in a system of linear equations for $S_{1,1}, S_{1,2}, \ldots, S_{1,n+1}$, which can be solved for a given value of H, realizing that $S_{1,n+1} = 0$ on the basis that the series $S_{1,n}$ converges to zero if the summation index n is significantly large. The remaining n linear equations containing the n unknown $S_{1,1}, S_{1,2}, \ldots, S_{1,n}$ can be solved numerically.

7. Determination of resistance coefficient corrections

The vector of force and torque about the particle centre exerted by the liquid flow on the particle are determined by the following closed integrals over the particle surface (Happel and Brenner, 1965b):

$$\mathbf{F} = \oiint_S \mathbf{P}\cdot d\mathbf{S} \tag{70}$$

$$T = \oiint_S \mathbf{R}\times(\mathbf{P}\cdot d\mathbf{S}) \tag{71}$$

where $d\mathbf{S}$ is a vector of surface area element, pointing into the liquid, and $\mathbf{R}$ is a vector related to the particle centre. The pressure tensor, $\mathbf{P}$, of the liquid flow is defined by

$$\mathbf{P} = -\mathbf{I}p + \mu[\nabla w + (\nabla w)^{\dagger}]$$

where $\mathbf{I}$ is the unit tensor and $(\nabla w)^{\dagger}$ is the transpose of the dyadic ∇w. Eqs. (70) and (71) in terms of the basic variables of the system depicted in Fig. 2 can be expressed by

$$\begin{aligned} F_l = UG_lR^2\mu\int_0^{2\pi}\int_0^{2\pi}\Bigg\{&\sin\theta\left[\left\{2\frac{\partial\beta}{\partial r}-\lambda\right\}\cos^2\varphi-\left(\frac{\partial\gamma}{\partial r}-\frac{\beta+\gamma}{r}\right)\sin^2\varphi\right] \\ &-\left[\left(\frac{\partial\varepsilon}{\partial r}+\frac{\partial\beta}{\partial z}\right)\cos^2\varphi-\left(\frac{\partial\gamma}{\partial z}-\frac{\varepsilon}{r}\right)\sin^2\varphi\right]\cos\theta\Bigg\}\sin\theta\,d\theta\,d\varphi \end{aligned} \tag{72}$$

$$\begin{aligned} T_l = UG_lR^3\mu\int_0^{2\pi}\int_0^{2\pi}\Bigg\{&\cos\varphi\left[\left(\frac{\partial\varepsilon}{\partial z}-\frac{\partial\beta}{\partial r}\right)\sin 2\theta-\left(\frac{\partial\varepsilon}{\partial r}+\frac{\partial\beta}{\partial z}\right)\cos 2\theta\right] \\ &+\left[\left(\frac{\partial\gamma}{\partial r}-\frac{\beta+\gamma}{r}\right)\sin\theta\cos\theta-\left(\frac{\partial\gamma}{\partial z}-\frac{\varepsilon}{r}\right)\cos^2\theta\right]\sin\varphi\Bigg\}\sin\theta\,d\theta\,d\varphi \end{aligned} \tag{73}$$

where the subscript l is equal to 0, 1 and 2 as described in Eq. (14). Both Eqs. (72) and (73) can be further simplified using the continuity equation and the appropriate boundary conditions at the particle surface, which gives, after some manipulation,

$$F_l = \frac{\pi\mu U G_l c}{2}\int_{-1}^{1}\left[\frac{\lambda c\sinh\tau\sin\eta}{(\cosh\tau-\sigma)^3} - \frac{c\sin\eta}{(\cosh\tau-\sigma)^2}\frac{\partial\lambda}{\partial\xi} - \frac{2}{\cosh\tau-\sigma}\frac{\partial\alpha_0}{\partial\xi}\right]\mathrm{d}\sigma \tag{74}$$

$$T_l = \pi\mu U G_l c^2\int_{-1}^{1}\left[\frac{\sin\eta}{2}\left\{\frac{\partial(\lambda c\coth\tau+2\alpha_1)}{\partial\xi}+\frac{\lambda c\cosh\tau+2\alpha_1\sinh\tau}{\cosh\tau-\sigma}\right\} + (1-\sigma\cosh\tau)\times\left\{\frac{\partial\alpha_0}{\partial\xi}+\frac{\alpha_0\sinh\tau}{\cosh\tau-\sigma}\right\}\right]\frac{\mathrm{d}\sigma}{(\cosh\tau-\sigma)^2} \tag{75}$$

where $\sigma=\cos\eta$. Substituting the equations for λ, α_0 and α_1 into these equations and integrating gives

$$F_l = \pi\mu U R G_l\sqrt{2}\sinh\tau\sum_{n=0}^{\infty}\left\{C_{0,n}+S_{0,n}+(n^2+n)(C_{\lambda,n}+S_{\lambda,n})\right\}$$

$$T_l = \pi\mu U R^2 G_l\frac{\sqrt{2}}{3}\sinh^2\tau\sum_{n=0}^{\infty}[2+\mathrm{e}^{-2q_n\tau}]\{(n^2+n)(2S_{1,n}+S_{\lambda,n}\coth\tau)-(2n+1-\coth\tau)S_{0,n}\} + [2-\mathrm{e}^{-2q_n\tau}]\{(n^2+n)C_{\lambda,n}\coth\tau-(2n+1-\coth\tau)C_{0,n}\}$$

These equations can be compared to the appropriate Stokes equations for particles in the bulk phase, giving the following equations for the resistance coefficient factors, f_{shl} and t_{shl} ($l=0,1$ and 2),

$$f_{shl} \equiv -\frac{F_l}{6\pi\mu R W_l(h/R)} = \frac{\sqrt{2}}{6}\frac{\sinh\tau}{\cosh^l\tau}\sum_{n=0}^{\infty}\left\{C_{0,n}+(n^2+n)C_{\lambda,n}\right\} \tag{76}$$

$$g_{shl} \equiv \frac{T_l}{8\pi\mu R^2 W_l(h)} = -\frac{\sinh^2\tau}{12\sqrt{2}\cosh^l\tau}\sum_{n=0}^{\infty}[4+2\mathrm{e}^{-2q_n\tau}](n^2+n)S_{1,n} + [2-\mathrm{e}^{-2q_n\tau}]\left\{(n^2+n)C_{\lambda,n}\coth\tau-(2n+1-\coth\tau)C_{0,n}\right\} \tag{77}$$

where h is the z coordinate of the particle centre (Fig. 2) and can be described by

$$h = H + R = R\cosh\tau$$

8. Results and discussion

8.1. Individual resistance functions

The numerical results for the resistance functions, f_{sh0}, g_{sh0}, f_{sh1}, g_{sh1}, f_{sh2} and g_{sh2} predicted by Eqs. (76) and (77) are shown in Figs. 3–5. For the large separation distance, the resistance functions for the forces are approximately equal to unity, showing insignificant influence of the interfaces on the forces, as expected for distant particles and bubbles. At large distances, the flow is uniform, resulting in zero torque on the particles. However, as the separation distance decreases,

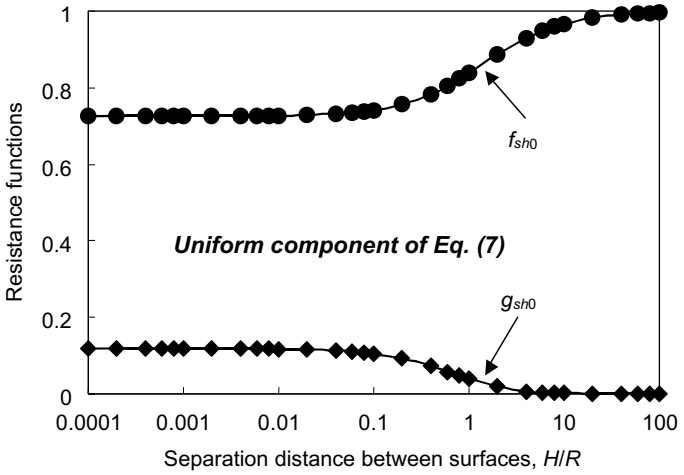

Fig. 3. Resistance functions for force and torque due to the uniform component of the shear flow.

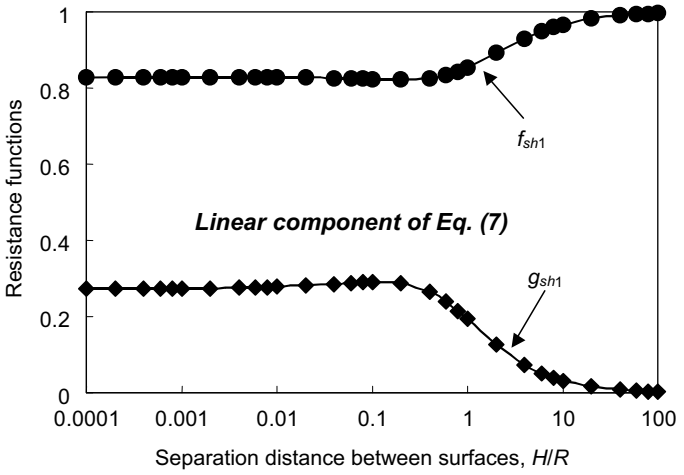

Fig. 4. Resistance functions for force and torque due to the linear component of the shear flow.

both the resistance functions for the force and torque deviate from unity and zero, respectively, due to the influence of the interfaces. The important difference between the results obtained for the slip gas–liquid interface in this paper and the results obtained for the solid rigid surface (Goren and O'Neill, 1971) is that the slip gas–liquid interface reduces the resistance functions for the force due to the uniform and linear shear flows. The drag force of the shear flows on particles at the slip gas–liquid interface is therefore smaller than in the liquid phase far from the interface.

8.2. Force of liquid shear flow on sliding particles

Due to the system asymmetry a particle in the shear flow in the tangential direction is subjected to both the translational and rotational motions. The translation also generates a torque about

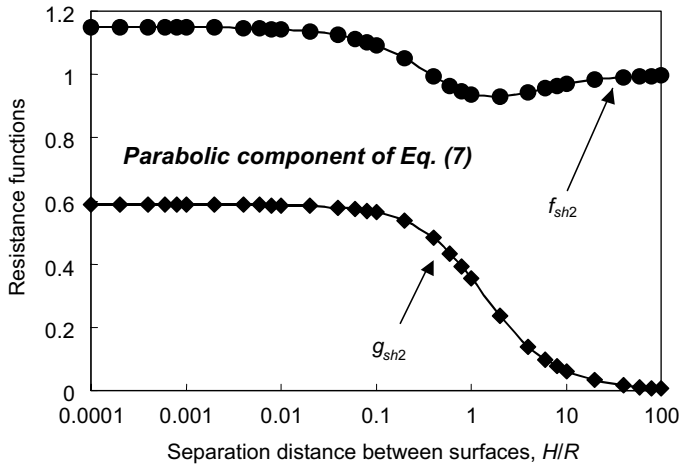

Fig. 5. Resistance functions for force and torque due to the parabolic component of the shear flow.

the particle centre and the rotation creates an additional drag force. The sum of the translational (tran), rotational (rot) and shear (sh) contributions allows for the drag (F_θ) and torque (T) on a particle to be described by

$$F_\theta = -6\pi\mu R V_\theta f_{\text{tran}} + 6\pi\mu\Omega R^2 f_{\text{rot}} + 6\pi\mu R(W_0 f_{\text{sh0}} + W_1 f_{\text{sh1}} + W_2 f_{\text{sh2}}) \tag{78}$$

$$T = 8\pi\mu R^2 V_\theta g_{\text{tran}} - 8\pi\mu\Omega R^3 g_{\text{rot}} + 8\pi\mu R^2(W_0 g_{\text{sh0}} + W_1 g_{\text{sh1}} + W_2 g_{\text{sh2}}) \tag{79}$$

where Ω is the angular velocity. W_0, W_1 and W_2 are the uniform, linear and parabolic terms of the shear flow velocity, i.e., $W = W_0 + W_1 + W_2$, which are described by Eq. (14). f_{tran} and f_{rot} describe the hydrodynamic resistance functions due to the translational and rotational forces on a particle translating in a stationary liquid. g_{tran} and g_{rot} describe the hydrodynamic resistance functions due to the torques of the translational and rotational contributions on a particle rotating in a stationary liquid. f_{sh0}, f_{sh1} and f_{sh2} describing the hydrodynamic resistance functions due to the forces of the linear and parabolic terms of the shear velocity on a stationary particle are given by Eq. (76). g_{sh0}, g_{sh1} and g_{sh2} describing the hydrodynamic resistance functions due to the torques of the linear and parabolic terms of the shear velocity on a stationary particle are determined by Eq. (77).

For sliding particles the combined torque must be balanced by the particle internal reaction, leading to $T = 0$, which gives

$$\Omega R = V_\theta \frac{g_{\text{tran}}}{g_{\text{rot}}} + \frac{W_0 g_{\text{sh0}} + W_1 g_{\text{sh1}} + W_2 g_{\text{sh2}}}{g_{\text{rot}}} \tag{80}$$

Substitution of Eq. (80) into Eq. (78) and comparing with Eq. (2) yields

$$f_3 = f_{\text{tran}} - f_{\text{rot}} \frac{g_{\text{tran}}}{g_{\text{rot}}} \tag{81}$$

$$f_4 = \frac{W_0 f_{40} + W_1 f_{41} + W_2 f_{42}}{W_0 + W_1 + W_2} \tag{82}$$

where

$$f_{40} = f_{sh0} + g_{sh0}\frac{f_{rot}}{g_{rot}} \tag{83}$$

$$f_{41} = f_{sh1} + g_{sh1}\frac{f_{rot}}{g_{rot}} \tag{84}$$

$$f_{42} = f_{sh2} + g_{sh2}\frac{f_{rot}}{g_{rot}} \tag{85}$$

The resistance functions, f_{rot} and g_{rot} can also be determined from the Stokes equation. The results for f_{rot} and g_{rot} for a particle rotating parallel to a slip gas–liquid interface are shown in Fig. 6. This problem will be dealt with in further detail elsewhere.

Now knowing f_{rot}, g_{rot}, f_{sh0}, g_{sh0}, f_{sh1}, g_{sh1}, f_{sh2} and g_{sh2} as a function of the separation distance we can determine the force correction factors described by Eqs. (83)–(85) for sliding particles. The results are shown in Fig. 7. Clearly, the influence of the shear flow on the resistance is different for the uniform, linear and parabolic shear components. In all cases, the force correction factors approach unity in the limit of large separation distances. However, as the separation approaches zero, the correction factors deviate from unity, approaching different constant values of 0.74, 0.85 and 1.20 for the uniform, linear and parabolic shear flows, respectively.

For the bubble–particle interaction modelling exercises, the numerical data for the force correction factors as a function of the separation distance, H/R, can be better replaced by simple approximate equations. As can be seen from Fig. 7, these functions approach the finite values at $H/R = 0$, and unity when H/R is very large. Based on these asymptotes, simple approximations for the force correction factors are expected to have the functional dependence of the form $(a + H/R)/(b + H/R)$. The numerical constants a and b can be obtained by the best fit to the numerical data shown in Fig. 7. The best fit was solved by the non-linear least squares procedure,

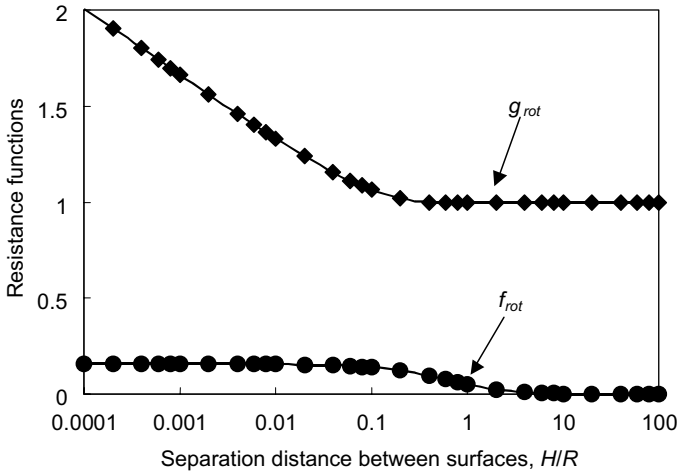

Fig. 6. Resistance functions for force and torque on a particle rotating parallel to a slip gas–liquid interface.

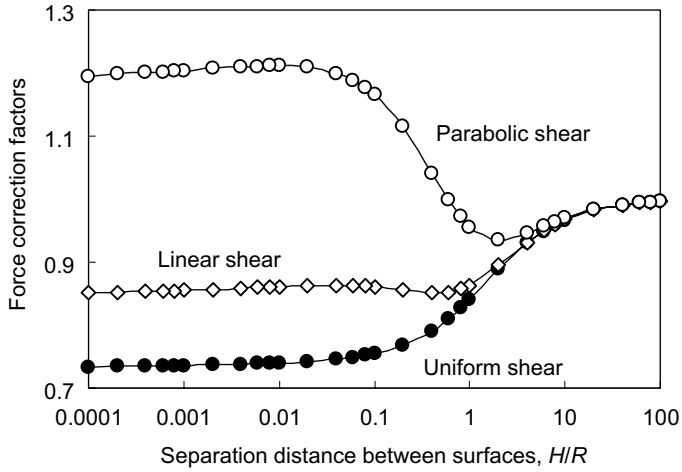

Fig. 7. Correction factors for the force of liquid shear flow on particles sliding over a slip gas–liquid interface: f_{40}, uniform component; f_{41}, linear component; and f_{42}, parabolic component.

which uses a quasi-Newton algorithm, with a forward difference scheme and a linear extrapolation to obtain initial estimates from a tangent vector, at each iteration to determine the direction to search. The resultant approximate expressions for the force correction factors as a function of H/R can be described by

$$f_{40} = \frac{1.107 + H/R}{1.502 + H/R} \tag{86}$$

$$f_{41} = \frac{3.676 + H/R}{4.304 + H/R} \tag{87}$$

$$f_{42} = \frac{0.166 + H/R}{0.136 + H/R} \tag{88}$$

These equations represent the global rational approximations for the force correction factors for the whole range of the separation distance.

It is also interesting to note that when the separation distance is significantly small, the drag force correction factors approach constants values. The asymptotic value is smaller than unity in the case of the uniform and linear shear flows, while it is greater than one for the parabolic shear flow. The individual asymptotic behaviours of the correction factors reflect the nature of the slip boundary conditions used at the gas–liquid interface. If the interface is no-slip, the drag forces and the force correction factors asymptotically increases to infinity. It will be important to investigate the situation when the particle comes into contact with the interface, with different wetting (contact angle) properties. We will address this problem in a forthcoming paper.

As described in the Section 1, the gas–liquid interface may be deformed during the bubble–particle attachment interaction. However, this deformation strongly depends on angle and magnitude of the bubble–particle approach velocity. If a particle approaches a bubble in the direction normal

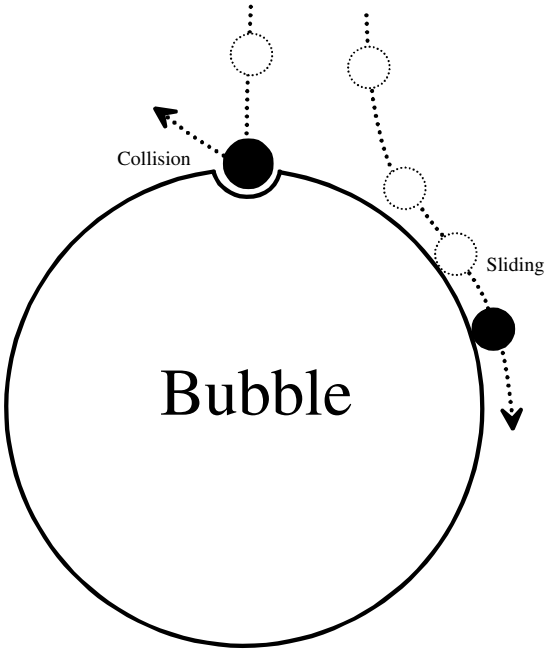

Fig. 8. Illustration of the collision and sliding attachment interaction between particles and bubbles in flotation.

to the bubble surface, the momentum of the approach is high, causing strong deformation of the local gas–liquid interface (Fig. 8). This bubble–particle interaction is called the collision attachment interaction and is significant for coarse particle flotation. The deformation of the gas–liquid interface is negligibly small (Schulze, 1989) for the particle size of about 50–100 μm and the bubble size of about 1–2 mm which are typically encountered in the flotation separation process. For these particles and bubbles, the attachment is governed by the sliding interaction and the gas–liquid interface can be locally planar in comparison to the curvature of the particle surface, which is described in this paper. For the coarse particle flotation, the theory presented in this paper requires a modification to consider the local deformation of the gas–liquid interface as the curvature of the local gas–liquid interface is compatible to the curvature of the particle surface and will influence the hydrodynamic interaction at short separation distances.

9. Conclusions

A mathematical model was developed to describe the hydrodynamic forces and torques on a fine solid sphere due to shear flows parallel to a slip surface of a rising air bubble. The liquid shear flow close to the bubble surface was determined using a Taylor series expansion and the numerical data obtained from the Navier–Stokes equation using CFD code FLUENT. The shear flow has three major components, corresponding to the uniform, linear and parabolic shear flows. The disturbance shear flows due to the particle were determined from the full Stokes equations described using the local cylindrical. The Stokes equations were solved for the velocity components and

pressure using the infinite series described in terms of the bispherical coordinates. The integration constants were determined from the no-slip boundary conditions at the particle surface and the slip boundary conditions at the gas–liquid interface, which produced a linear system of algebraic equations. The system of algebraic equations was solved numerically assuming that the integration constants converge to zero if the summation index of the infinite series is significantly large. The integration constants were then used to determine the resistance forces and torques on the particle. The force and torque equations were compared to the Stokes equation for the drag force and the equation for the torque in the bulk phase to obtain the resistance functions, which describe the deviations as functions of the separation distance between the particle and bubble surfaces. For sliding particles the resultant torque is balanced, allowing the angular velocity to be determined. The force correction factors for sliding particles were determined as functions of the separation distance. Finally, rational approximate expressions are presented for the force correction factors, which are in good agreement with the exact numerical result and can be readily applied to the bubble–particle modelling exercises.

Acknowledgement

The authors gratefully acknowledge the Australian Research Council for financial support.

References

Batchelor, G.K., 1972. Sedimentation in a dilute suspension of spheres. J. Fluid Mech. 52, 245–268.

Clift, R., Grace, J.R., Weber, M.E., 1978. Bubbles, Drops and Particles. Academic Press, New York, 380 pp.

Dai, Z., Fornasiero, D., Ralston, J., 2000. Particle–bubble collision models—a review. Adv. Colloid Interface Sci. 85, 231–256.

Dobby, G.S., Finch, J.A., 1986. A model of particle sliding time for flotation size bubbles. J. Colloid Interface Sci. 109, 493–498.

Dobby, G.S., Finch, J.A., 1987. Particle size dependence in flotation derived from a fundamental model of the capture process. Int. J. Miner. Process. 21, 241–260.

Goldman, A.J., Cox, R.G., Brenner, H., 1967a. Slow viscous motion of a sphere parallel to a plane wall I. Motion through a quiescent fluid. Chem. Eng. Sci. 22, 637–651.

Goldman, A.J., Cox, R.G., Brenner, H., 1967b. Slow viscous motion of a sphere parallel to a plane wall II. Couette flow. Chem. Eng. Sci. 22, 653–660.

Goren, S.L., O'Neill, M.E., 1971. Hydrodynamic resistance to a particle of a dilute suspension when in the neighborhood of a large obstacle. Chem. Eng. Sci. 26, 325–338.

Happel, J., Brenner, H., 1965a. Low Reynolds Number Hydrodynamics. Prentice Hall, Englewood Cliffs, NJ, 438 pp.

Happel, J., Brenner, H., 1965. Low Reynolds number hydrodynamics with special applications to particulate media. Prentice-Hall International Series in the Physical and Chemical Engineering Sciences, 553 pp.

Jameson, G.J., Nam, S., Young, M.M., 1977. Physical factors affecting recovery rates in flotation. Miner. Sci. Eng. 9, 103–118.

Magnus, W., Oberhettinger, F., Soni, R.P., 1966. Formulas and Theorem for Special Functions of Mathematical Physics. Springer-Verlag, New York, 476 pp.

Moore, D.W., 1963. The boundary layer on a spherical gas bubble. J. Fluid Mech. 16, 161–176.

Nguyen, A.V., 1993. On the sliding time in flotation. Int. J. Miner. Process. 37, 1–25.

Nguyen, A.V., 1994. The collision between fine particles and single air bubbles in flotation. J. Colloid Interface Sci. 162, 123–128.

Nguyen, A.V., 1999. Hydrodynamics of liquid flows around air bubbles in flotation: a review. Int. J. Miner. Process. 56, 165–205.

Nguyen, A.V., Evans, G.M., 2002. Axisymmetric approach of a solid sphere toward a non-deformable planar slip interface in the normal stagnation flow—development of global rational approximations for resistance coefficients. Int. J. Multiphase Flow 28, 1369–1380.

Nguyen, A.V., Evans, G.M., 2004. Exact and global rational approximate expressions for resistance coefficients for a colloidal solid sphere moving in a quiescent liquid parallel to a slip gas–liquid interface. J. Colloid Interface Sci. 273, 262–270.

Schulze, H.J., 1983. Physico-Chemical Elementary Processes in Flotation. In: Fuerstenau, D.W. (Ed.), Developments in Mineral Processing, vol. 4. Elsevier, Amsterdam, p. 320.

Schulze, H.J., 1989. Hydrodynamics of bubble–mineral particle collisions. Miner. Process. Extract. Met. Rev. 5, 43–76.